Ground State Potential Energy Curve and Dissociation Energy of MgH†

Alireza Shayesteh,‡ Robert D. E. Henderson, Robert J. Le Roy, and Peter F. Bernath*,§

Department of Chemistry and Department of Physics and Astronomy, University of Waterloo, Waterloo, Ontario, Canada N2L 3G1

Received: July 20, 2007; In Final Form: September 21, 2007

New high-resolution visible emission spectra of the MgH molecule have been recorded with high signal-to-noise ratios using a Fourier transform spectrometer. Many bands of the $A\ ^2\Pi \rightarrow X\ ^2\Sigma^+$ and $B'\ ^2\Sigma^+ \rightarrow X\ ^2\Sigma^+$ electronic transitions of ^{24}MgH were analyzed; the new data span the $v' = 0-3$ levels of the $A\ ^2\Pi$ and $B'^2\Sigma^+$ excited states and the $v'' = 0-11$ levels of the $X\ ^2\Sigma^+$ ground electronic state. The vibration−rotation energy levels of the perturbed $A\ ^2\Pi$ and $B'\ ^2\Sigma^+$ states were fitted as individual term values, while those of the $X\ ^2\Sigma^+$ ground state were fitted using the direct-potential-fit approach. A new analytic potential energy function that imposes the theoretically correct attractive potential at long-range, and a radial Hamiltonian that includes the spin-rotation interaction were employed, and a significantly improved value for the ground state dissociation energy of MgH was obtained. The $v'' = 11$ level of the $X\ ^2\Sigma^+$ ground electronic state was found to be the highest bound vibrational level of ^{24}MgH, lying only about 13 cm^{-1} below the dissociation asymptote. The equilibrium dissociation energy for the $X\ ^2\Sigma^+$ ground state of ^{24}MgH has been determined to be $D_e = 11104.7 \pm 0.5$ cm^{-1} (1.37681 ± 0.00006 eV), whereas the zero-point energy ($v'' = 0$) is 739.11 ± 0.01 cm^{-1}. The zero-point dissociation energy is therefore $D_0 = 10365.6 \pm 0.5$ cm^{-1} (1.28517 ± 0.00006 eV). The uncertainty in the new experimental dissociation energy of MgH is more than 2 orders of magnitude smaller than that for the best value available in the literature. MgH is now the only hydride molecule other than H_2 itself for which all bound vibrational levels of the ground electronic state are observed experimentally and for which the dissociation energy is determined with subwavenumber accuracy.

Introduction

The first laboratory spectrum of MgH was photographed a century ago in an effort to identify strong bands appearing in sunspot spectra.[1,2] MgH has become an important molecule in astrophysics because its visible bands appear strongly in the absorption spectra of the sun and of some cool stars[3−5] and are used routinely to estimate the magnesium isotope abundances.[6,7] The first series of spectroscopic studies on MgH were carried out in the 1920s and 1930s, shortly after the development of quantum mechanics, and several electronic transitions involving the $X\ ^2\Sigma^+$ ground electronic state and the low-lying excited states were observed and analyzed.[8−16] The strongest bands of MgH are from the $A\ ^2\Pi - X\ ^2\Sigma^+$ system, which involves the transition of an unpaired electron between nonbonding π and σ orbitals. A complete summary of the MgH studies prior to 1977 has been compiled by Huber and Herzberg.[17]

The visible and ultraviolet spectra of MgH and MgD were studied extensively by Balfour and co-workers in the 1970s.[18−25] A value for the dissociation energy of MgH in the $X\ ^2\Sigma^+$ ground state was first obtained by Balfour who found it to be $D_0 = 1.33 \pm 0.06$ eV, based on a Birge−Sponer extrapolation from the $v'' = 6$ level observed in the $A\ ^2\Pi \rightarrow X\ ^2\Sigma^+$ spectrum.[18] A few years later, Balfour and Lindgren obtained a refined D_0 value of 1.27 ± 0.03 eV, this time from the limiting curve of dissociation up to the $v'' = 9$ level observed in the $B'\ ^2\Sigma^+ \rightarrow X\ ^2\Sigma^+$ spectrum.[24] Bernath et al. recorded the $A\ ^2\Pi \rightarrow X\ ^2\Sigma^+$ emission spectrum of MgH at very high resolution using a Fourier transform spectrometer,[26] and predicted highly accurate vibration−rotation and pure rotational transition frequencies for the $X\ ^2\Sigma^+$ ground state. Soon after their work, the diode-laser-infrared and the microwave spectra of MgH were recorded and analyzed.[27−31] More recently, Fourier transform infrared emission spectra of MgH and MgD were obtained in our laboratory at the University of Waterloo, and a combined-isotopologue analysis of the infrared and microwave data was performed using a Dunham-type energy level expression.[32]

Parallel to the experimental work on MgH, several theoretical studies were carried out in the 1970s. The equilibrium internuclear distance, vibrational frequencies, dissociation energies, and dipole moments of MgH have been computed by various ab initio theoretical methods, and the experimental assignments of the low-lying excited states have been confirmed.[33−37] Due to its importance in astrophysics, the line and continuum opacities of MgH in cool stellar atmospheres were computed recently by Kirby and co-workers.[38−41] The current best ab initio value[33] for the dissociation energy of MgH, $D_0 = 1.25$ eV, is in good agreement with the experimental value of Balfour and Lindgren.[24]

This paper reports new high-resolution emission spectra of the $A\ ^2\Pi \rightarrow X\ ^2\Sigma^+$ and $B'\ ^2\Sigma^+ \rightarrow X\ ^2\Sigma^+$ transitions of MgH. The new data span the $v = 0-11$ levels of the $X\ ^2\Sigma^+$ ground state of MgH and have been combined with the infrared and microwave data available in the literature. A direct-potential-fit was performed for the $X\ ^2\Sigma^+$ ground state, and the $v = 11$ level was found to be the highest bound vibrational level. This

† Part of the "Giacinto Scoles Festschrift".

* To whom correspondence should be addressed. E-mail: pfb500@york.ac.uk. Fax: +44-1904-432516. Phone: +44-1904-434526.

‡ Current address: Department of Chemistry, York University, Toronto, Ontario, Canada M3J 1P3.

§ Current address: Department of Chemistry, University of York, Heslington, York, U.K., YO10 5DD.

10.1021/jp075704a CCC: $37.00
Published on Web 11/20/2007

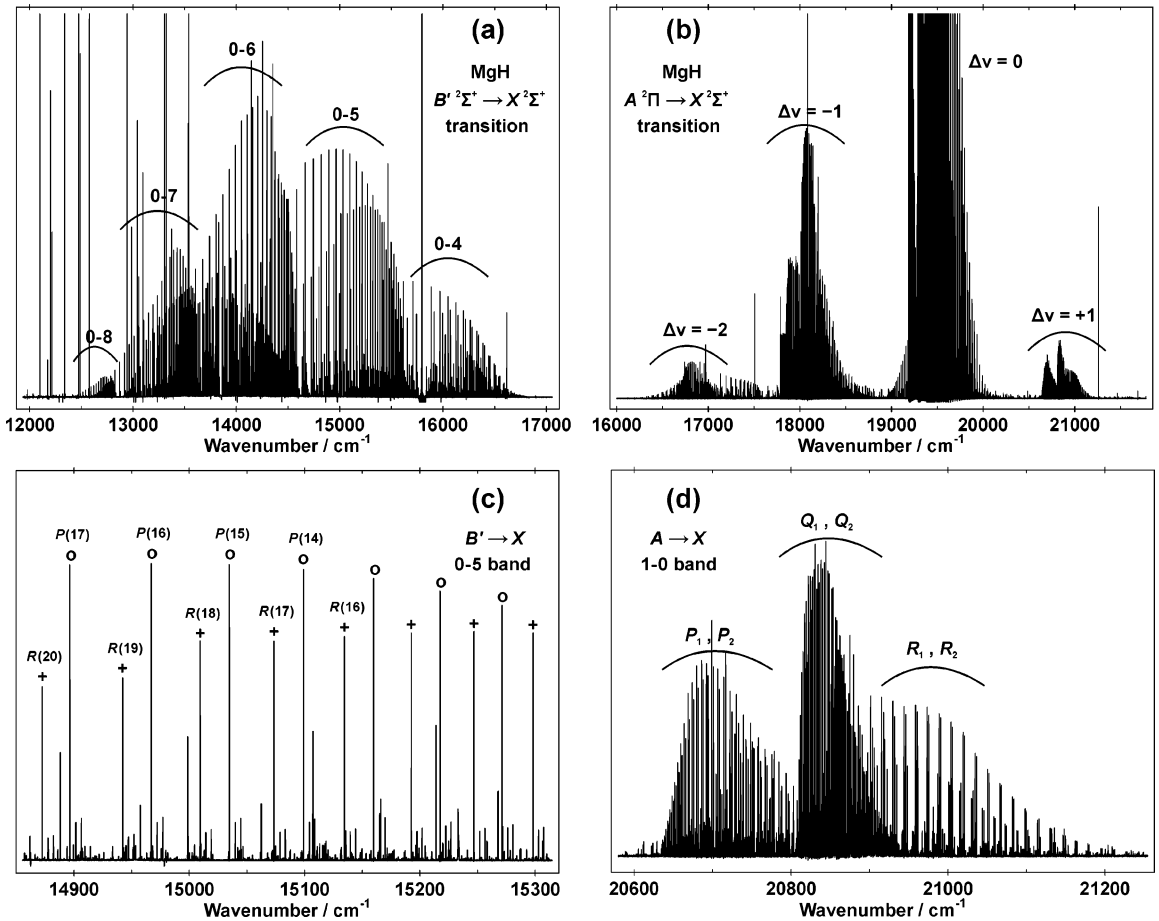

Figure 1. (a) Overview of the $B'\,^2\Sigma^+ \rightarrow X\,^2\Sigma^+$ spectrum of MgH, showing the $v' = 0$ progression. (b) An overview of the $A\,^2\Pi \rightarrow X\,^2\Sigma^+$ spectrum with $\Delta v = -2$ to $+1$ sequences; the $\Delta v = 0$ lines are very strong and their intensities continue beyond the vertical scale of this figure. (c) Rotational structure, *P* and *R* branches, in the 0−5 band of the $B' \rightarrow X$ spectrum. (d) The 1−0 band of the $A \rightarrow X$ spectrum with six strong branches.

fit resulted in a significantly improved value for the ground state dissociation energy of MgH, with an uncertainty some 2 orders of magnitude smaller than the one reported by Balfour and Lindgren,[24] which was the best value available in the literature.

Experiment and Results

The discharge-furnace emission source described in ref 32 was used to generate the visible spectra of MgH. Approximately 50 grams of magnesium powder was placed directly inside an alumina tube, and heated to about 550−650 °C. The tube was sealed with CaF_2 windows and evacuated using a rotary pump. A mixture of argon (1.6 Torr) and hydrogen (0.2 Torr) flowed slowly through the cell, and a dc discharge was created between stainless-steel electrodes placed in each end of the tube. Emission from the source was focused by a CaF_2 lens onto the entrance aperture of a Bruker IFS 120 HR Fourier transform spectrometer, and the signal was detected by a silicon photodiode detector.

Two emission spectra of MgH were recorded: the first one was recorded at 650 °C with an instrumental resolution of 0.0375 cm^{-1}, and the spectral range was limited to 9000−18000 cm^{-1} by the detector response and by using a 550 nm long-wave-pass filter. The second spectrum was recorded at 550 °C with an instrumental resolution of 0.065 cm^{-1}, and the spectral bandpass was set to 16 000−23 000 cm^{-1} by using 450 nm long-wave-pass and 600 nm short-wave-pass filters. The signal-to-noise ratios (S/N) were improved by co-adding a few hundred scans during several hours of recording (220 and 400 scans for the first and second spectrum, respectively). The resulting S/N values were about 1000 for the strongest emission lines of MgH. The first MgH spectrum (9000−18 000 cm^{-1}) contained mostly emission lines from the $B'\,^2\Sigma^+ \rightarrow X\,^2\Sigma^+$ transition, whereas the strongest emission lines in the second spectrum (16 000−23 000 cm^{-1}) were from the $A\,^2\Pi \rightarrow X\,^2\Sigma^+$ transition; see Figure 1.

Line positions were measured using the program WSpectra written by Carleer (Université Libre de Bruxelles). Since the spectrometer was not operated under vacuum, an air−vacuum correction was performed using the formula given in ref 42, and the absolute wavenumber scales of the spectra were also calibrated. The $B'\,^2\Sigma^+ \rightarrow X\,^2\Sigma^+$ spectrum (9000−18 000 cm^{-1}) was calibrated using argon atomic lines reported by Norlen.[43] The $A\,^2\Pi \rightarrow X\,^2\Sigma^+$ spectrum (16 000−23 000 cm^{-1}) was calibrated against an older high-resolution MgH spectrum recorded by Bernath et al.,[26] which was also calibrated using argon atomic lines. According to a recent paper on the argon atomic emission lines in a hollow-cathode discharge lamp,[44] the line positions of Norlen[43] should be multiplied by the factor $[1 + 67 \times 10^{-9}]$. We also multiplied our calibrated line positions by this factor, to make them consistent with the most recent measurements of argon atomic lines.[44] The absolute accuracy of our calibrated line positions is better than 0.005 cm^{-1} for unblended lines.

Our spectra contain several rovibronic bands of the $A\,^2\Pi \rightarrow X\,^2\Sigma^+$ and $B'\,^2\Sigma^+ \rightarrow X\,^2\Sigma^+$ systems for ^{24}MgH, ^{25}MgH, and ^{26}MgH, but only the data for the major isotopologue, ^{24}MgH, have been assigned and analyzed in the present work. For both $A\,^2\Pi$ and $B'\,^2\Sigma^+$ excited states, bands involving $v' = 0-3$ were

TABLE 1: Observed Bands in the New $A^2\Pi \rightarrow X\ ^2\Sigma^+$ and $B'\ ^2\Sigma^+ \rightarrow X\ ^2\Sigma^+$ Spectra of ^{24}MgH[a]

		$A^2\Pi$				$B'\ ^2\Sigma^+$			
		$v' = 0$	$v' = 1$	$v' = 2$	$v' = 3$	$v' = 0$	$v' = 1$	$v' = 2$	$v' = 3$
	$v'' = 0$	vs	s						
	$v'' = 1$	s	vs	s				w	w
	$v'' = 2$	s	s	vs	s	s	s	s	s
	$v'' = 3$	w	s	s	s	s	s	s	s
	$v'' = 4$		w	s	s	s	s	s	w
$X\ ^2\Sigma^+$	$v'' = 5$			w	w	s	s	w	w
	$v'' = 6$				w	s	s	s	s
	$v'' = 7$					s	s	w	w
	$v'' = 8$					s	s	s	w
	$v'' = 9$					w	s	s	s
	$v'' = 10$						w	w	w
	$v'' = 11$								w

[a] The acronyms "vs", "s", and "w" stand for "very strong", "strong", and "weak", respectively. The $v'' = 10$ and 11 levels had not been observed in the previous studies of MgH.

assigned. The B_v values of the $A^2\Pi$ state vibrational levels are slightly larger than those of the corresponding levels for the $X\ ^2\Sigma^+$ state, so that most of the $A \rightarrow X$ bands have *P*-heads. On the other hand, the B_v values of the $B'\ ^2\Sigma^+$ state vibrational levels are significantly smaller than those of the corresponding levels for the $X\ ^2\Sigma^+$ state, so that most of the $B' \rightarrow X$ bands have *R*-heads at low values of *N* (the rotational quantum number). The $A\ ^2\Pi \rightarrow X\ ^2\Sigma^+$ system consisted of $\Delta v = +1, 0, -1, -2$, and -3 sequences involving the $v'' = 0-6$ levels of the $X\ ^2\Sigma^+$ ground state. The diagonal Franck−Condon factors for the $A \rightarrow X$ system are significantly larger than the off-diagonal ones, so the $\Delta v = 0$ bands were the strongest in this system. In contrast, the potential energy curve of the $B'\ ^2\Sigma^+$ state has a distinctly different shape than that of the $X\ ^2\Sigma^+$ state, and many off-diagonal bands of the $B'\ ^2\Sigma^+ \rightarrow X\ ^2\Sigma^+$ transition, involving the $v'' = 1-11$ levels of the $X\ ^2\Sigma^+$ state, appeared strongly in our spectra. Together, the $A \rightarrow X$ and $B' \rightarrow X$ systems span the entire range of the $X\ ^2\Sigma^+$ ground state potential energy curve, i.e., the $v'' = 0-11$ vibrational levels. The highest vibrational level of the $X\ ^2\Sigma^+$ state observed in previous studies of MgH was the $v'' = 9$ level.[24] Table 1 lists all of the observed bands in the new MgH spectra.

The angular momentum coupling scheme of the $A^2\Pi$ state of MgH is a case intermediate between Hund's coupling cases (a) and (b). At large values of *J* (the total angular momentum quantum number), the $A^2\Pi$ state clearly resembles a Hund's case (b), whereas at low *J*'s, it is best described by a Hund's case (a) coupling scheme.[45] There were six strong branches for the $A^2\ \Pi \rightarrow X\ ^2\Sigma^+$ bands, P_1, Q_1, R_1, P_2, Q_2, and R_2, and some satellite branches, e.g., P_{12} and R_{21} were also observed. Rotational lines of the $B'\ ^2\Sigma^+ \rightarrow X\ ^2\Sigma^+$ bands showed a doublet splitting (the *e*/*f* spin components) due to the spin-rotation interaction, although the splitting was sometimes only partially resolved. For rotational lines in which the *e*/*f* splitting was not resolved, the observed line position was used for both *e* and *f* components, and a larger uncertainty (typically 0.015 cm^{-1}) was used. Most of the unblended lines were given an experimental uncertainty of 0.005 cm^{-1}.

There are several perturbations in the rotational levels of the $A^2\Pi$ and $B'\ ^2\Sigma^+$ excited states, due to accidental level-crossings between these states. Therefore, in order to obtain optimum spectroscopic constants for the $X\ ^2\Sigma^+$ state from these electronic transitions, the upper state energy levels were treated as individual term values. The previous MgH data from the high-resolution infrared and microwave spectra were also included in our data set. The infrared and microwave data have experimental uncertainties of 10^{-3} and 10^{-5} cm^{-1}, respectively, and were taken directly from our recent MgH paper.[32] The high quality infrared and microwave data (for $v'' = 0$ to 4 of the $X\ ^2\Sigma^+$ state) were useful for assignments of the electronic bands, especially for determining the absolute *e*/*f* parity assignments of the $B' \rightarrow X$ bands involving the $v'' = 2-4$ levels. The rotational assignments of the bands with $v'' > 4$ were based on combination differences of the lower or upper states. A complete list of all experimental data for ^{24}MgH (~7000 line positions) and the results of our data analysis are presented in Tables 1S−9S, provided as Supporting Information.

The $B'\ ^2\Sigma^+ \rightarrow X\ ^2\Sigma^+$ bands provided information on very high vibrational and rotational levels of the $X\ ^2\Sigma^+$ ground state; for example, rotational lines of the 0−2 band were observed up to $N'' = 48$. The $v'' = 2$, $N'' = 48$ level is called "quasibound" because it lies above the dissociation asymptote (by more than 3000 cm^{-1}) but below the centrifugal barrier maximum. Numerous other quasibound levels were observed for the higher vibrational levels of the $X\ ^2\Sigma^+$ state. Quasibound levels are expected to be broadened due to the tunneling predissociation that reduces their lifetime. In some cases, the observed broadening was significantly larger than the Doppler broadening and could be measured by fitting the observed spectral line profile to the Voigt line shape function, a convolution of Gaussian and Lorentzian functions. The Gaussian width indicates the Doppler broadening, and the Lorentzian width is due to the natural lifetime broadening. The natural lifetime widths were measured in two steps. First, the temperature of MgH molecules inside the furnace-discharge source was estimated to be 1250 °C, from the Gaussian widths of about one thousand unblended lines. Then, the Lorentzian widths for the quasibound levels were fitted while the Gaussian widths were fixed to the calculated Doppler broadening at this temperature. Table 2 lists energies of the highest observed N'' levels for each vibrational quantum number, and the tunneling predissociation widths for those that are quasibound. These lifetime widths were included as additional data in the direct-potential-fit analysis, as was done in ref 46. The broadening of the $(v'', N'') = (4, 40)$, (6, 31), and (8, 20) levels of the $X\ ^2\Sigma^+$ state are shown in expanded views of very small portions of the $B'\ ^2\Sigma^+ \rightarrow X\ ^2\Sigma^+$ spectrum in Figure 2. The spin-rotation splitting, lines from the minor isotopes of Mg, and some lines with $v'' = 10$ and 11 can also be seen in this figure.

Data Analysis

The ability of a set of parameters to reproduce the observed data accurately is represented by the dimensionless root-mean-square deviation of the fit, defined by[47]

TABLE 2: Highest Observed Rotational Quantum Numbers, N, in the Vibrational Levels of the $X\,^2\Sigma^+$ Ground State of ^{24}MgH, and the Tunneling Lifetime Widths[a]

v″	highest N'' [obs.]	$(E_{vN}-D_e)$/ cm^{-1}	width/ cm^{-1} [obs.]	width/ cm^{-1} [calc.]	highest N'' predicted[b]
0	42	−1090.3			61
1	40	−735.0			56
2	48	+3103.9		0.06	51
3	44	+2490.5		0.15	47
4	40	+1978.4	0.47	0.41	42
5	35	+1322.6	0.11	0.11	37
6	31	+1028.1	1.05	0.94	32
7	26	+645.3	1.15	1.14	27
8	20	+279.5	0.164	0.170	22
9	14	+88.5	0.05	0.05	15
10	8	+9.0		0.0008	9
11	3	−3.4			4

[a] The observed tunneling lifetime widths for the (v'', N'') = (4, 39), (6, 30), and (7, 25) levels are 0.024, 0.041, and 0.036 cm^{-1}, respectively. [b] The highest possible N'' for each vibrational level was calculated using the total potential energy function; see the text.

$$\overline{dd} = \left\{\frac{1}{n}\sum_{i=1}^{n}\left[\frac{y_{calc}(i)-y_{obs}(i)}{u(i)}\right]^2\right\}^{1/2} \quad (1)$$

In the above equation, n is the number of experimental data, $y_{obs}(i)$ is an observed transition wavenumber with an uncertainty of $u(i)$, and $y_{calc}(i)$ is a transition wavenumber predicted by the model. A fit of good quality should have $\overline{dd} \leq 1.0$, because larger values of $\overline{dd}$ indicate that the molecular model used is inadequate for reproducing the data within their experimental uncertainties. Due to the numerous perturbations in the $A^2\Pi$ and $B'\,^2\Sigma^+$ excited states, their vibration−rotation energy levels were fitted as individual term values in all steps of the present analysis. Molecular parameters for the $X\,^2\Sigma^+$ ground electronic state of ^{24}MgH were obtained from our complete data set using the two approaches described below.

A. Empirical Parameter Fit. In the first steps of analysis, an empirical band-constant fit was performed for the $X\,^2\Sigma^+$ ground state, yielding an independent vibrational origin, G(v), inertial rotational constant, B_v, and a set of centrifugal distortion constants, D_v, H_v, L_v, M_v, etc., for each observed vibrational level ($v'' = 0-11$). The rotational energy for each vibrational level was fitted to a polynomial in $[N(N+1)]$, where N is the rotational quantum number for a $^2\Sigma^+$ state

$$E_v(N) = \sum_{m=0} K_v^{(m)}[N(N+1)]^m = G_v + B_v[N(N+1)] - D_v[N(N+1)]^2 + H_v[N(N+1)]^3 + \cdots \quad (2)$$

In addition, the following Dunham-type energy expression, in which $s(e;N) = +N/2$ and $s(f;N) = -(N+1)/2$, was added to eq 2 to take the spin-rotation interaction into account.[32]

$$E_{Spin-Rot}(v,N) = s(e/f;N) \times \sum_{l=0}\sum_{m=1}\gamma_{l,m}\left(v+\frac{1}{2}\right)^l [N(N+1)]^{m-1} \quad (3)$$

This band-constant fit required a large number of centrifugal distortion constants for most vibrational levels, mainly because the data span a very large range of N values and many quasi-bound levels were observed. For example, for the $v'' = 2-6$ levels, the rotational energy had to be expressed by a ninth-order power series in $[N(N+1)]$. The band constants for the $v'' = 0-11$ levels, which are listed in Table 4S, can reproduce the observed energy levels of the $X\,^2\Sigma^+$ ground state within the experimental uncertainty. However, we emphasize that these band constants are merely empirical coefficients of polynomials in $[N(N+1)]$, and most of the high-order centrifugal distortion constants have no physical significance. Only the leading constants, G(v), B_v, and D_v are listed in Table 3. The band-constant fit is obviously not the best method of data reduction, but it proved to be very useful for confirming the rotational assignments of all of the observed transitions. Figure 3 shows plots of ΔG(v) and B_v for the $X\,^2\Sigma^+$ ground state of ^{24}MgH.

A second type of empirical fit to the vibration−rotation energy levels of the $X\,^2\Sigma^+$ state was performed by replacing eq 2 with the familiar Dunham level-energy expression[48,49]

$$E(v,N) = \sum_{l,m} Y_{l,m}\left(v+\frac{1}{2}\right)^l [N(N+1)]^m \quad (4)$$

In principle, the Dunham fit should require fewer parameters than does the band-constant fit, because it links the constants of different vibrational levels through power series in $(v + {}^1/_2)$. It turned out, however, that very high-order Dunham coefficients were required in order to obtain a satisfactory fit, and the total number of parameters was even larger than that for the band-constant fit. The reason for this is the fact that the very wide range of vibrational and rotational levels observed in our spectra requires the use of unusually high-order polynomials in both $(v + {}^1/_2)$ and $[N(N+1)]$, and thus the Dunham parameters obtained in this fit have no physical significance. For both of these "parameter fits", band-constant and Dunham, more than 100 parameters were required to fully represent the $X\,^2\Sigma^+$ ground state energy levels, yielding $\overline{dd}$ values of 0.768 and 0.790, respectively.

B. Direct Potential Fit. The best method for spectroscopic data reduction is the direct-potential-fit (DPF) approach; it greatly reduces the number of parameters required to reproduce the data, and it directly provides a quantum-mechanically accurate physical model for the system. In the DPF analysis, the $X\,^2\Sigma^+$ ground electronic state of ^{24}MgH is described by an analytic potential energy function whose parameters are adjusted until the eigenvalues of the following radial Schrödinger equation match the observed vibration−rotation energy levels

$$\left\{\frac{-\hbar^2}{2\mu}\frac{d^2}{dr^2} + V_{ad}(r) + \frac{\hbar^2 N(N+1)}{2\mu r^2}[1+g(r)] + s(e/f;N)\Delta V_\Sigma(r)\right\}\psi_{v,N}(r) = E_{v,N}\psi_{v,N}(r) \quad (5)$$

The first term in the above Hamiltonian is the kinetic energy operator, in which μ is the reduced mass of ^{24}MgH. Since the only variable in eq 5 is the internuclear distance (r), exact numerical solutions of this Schrödinger equation can be computed for all vibrational levels associated with each value of the rotational quantum number N. The term $V_{ad}(r)$ is the rotationless adiabatic internuclear potential for ^{24}MgH. If more than one isotopologue was being considered, an atomic-mass-dependent correction function, $\Delta V_{ad}(r)$, would be added to the adiabatic potential. The third term in the Hamiltonian operator of eq 5 is the centrifugal potential $V_{cent}(r)$ due to the rotation of the molecule, in which $g(r)$ is a correction function that takes account of nonadiabatic Born−Oppenheimer breakdown effects. Finally, for the special case of $^2\Sigma^+$ electronic states, the term $\Delta V_\Sigma(r)$ is included to account for the spin-rotation interaction energy, where $s(e;N) = +N/2$ and $s(f;N) = -(N+1)/2$. Note

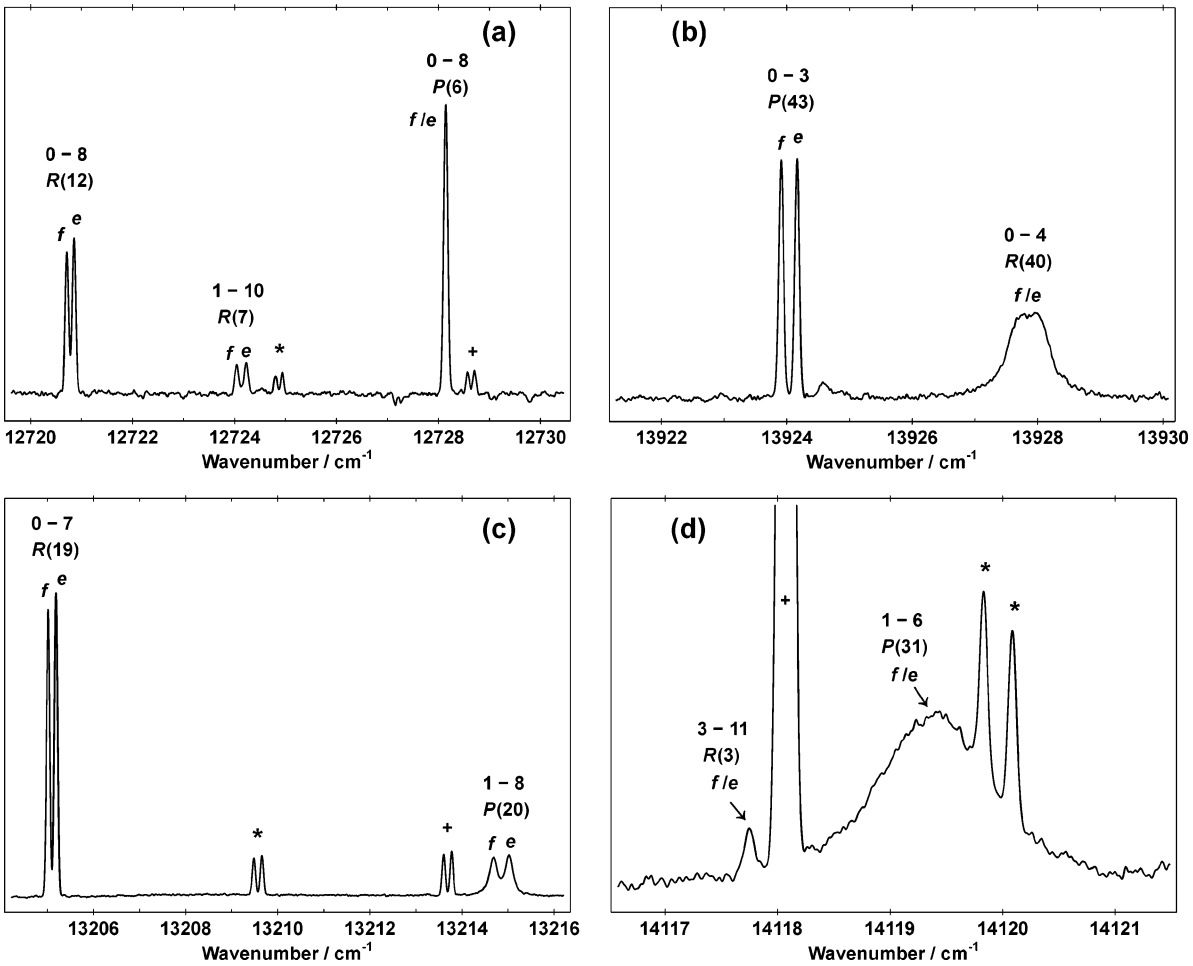

Figure 2. Expanded views of the $B'\,^2\Sigma^+ \rightarrow X\,^2\Sigma^+$ spectrum of MgH showing the *e*/*f* spin doubling in some rotational lines, and the energy level broadening of the $(v'', N'') = (4, 40)$, (6, 31), and (8, 20) levels of the $X\,^2\Sigma^+$ state. The weak lines marked with stars and crosses are from the minor isotopes of magnesium, ^{25}Mg and ^{26}Mg, respectively.

TABLE 3: Vibrational Energies, Inertial Rotational Constants, Centrifugal Distortion Constants, and the Turning Points for the Vibrational Levels of the $X\,^2\Sigma^+$ Ground State of ^{24}MgH[a]

v″	G_v/cm^{-1}	B_v/cm^{-1}	$10^4\,D_v$/cm^{-1}	r_{min}/Å	r_{max}/Å
0	739.1094	5.736508	3.543328	1.591	1.899
1	2171.0874	5.555289	3.557152	1.506	2.050
2	3539.7878	5.367551	3.600323	1.455	2.170
3	4841.4399	5.169787	3.689584	1.417	2.281
4	6070.4989	4.956644	3.854068	1.387	2.391
5	7218.7623	4.719638	4.147419	1.363	2.504
6	8273.9182	4.444650	4.675260	1.343	2.627
7	9217.1113	4.106852	5.670222	1.326	2.769
8	10018.7619	3.659651	7.716533	1.313	2.949
9	10631.8328	3.007412	12.63343	1.304	3.222
10	10988.5015	1.968707	26.55785	1.298	3.814
11	11091.3418	0.887068	42.20233	1.297	5.574

[a] All of the constants in this table have been calculated from the $MLR_4(6,18)$ potential function. The vibrational energies are relative to the bottom of the potential curve.

also that $V_{ad}(r)$, $\Delta V_\Sigma(r)$, and $E_{v,N}$ in eq 5 have units of energy, although it is customary to report them in wavenumber (cm^{-1}) units.

Two different analytic functions were used for the effective adiabatic internuclear potential: the expanded Morse oscillator $EMO_p(n_S, n_L)$, and the Morse/long-range $MLR_p(n_S, n_L)$ potentials. EMO functions are represented by the equation

$$V_{ad}(r) = V_{EMO}(r) = D_e[1 - e^{-\phi_{EMO}(r)\cdot(r-r_e)}]^2 \qquad (6)$$

in which D_e is the equilibrium dissociation energy and r_e is the equilibrium internuclear distance. An EMO potential is similar to the familiar Morse potential[50] but with the constant exponent coefficient of the Morse potential (β) replaced by the coefficient function $\phi_{EMO}(r)$. The dependence of $\phi_{EMO}(r)$ on the internuclear distance is via the dimensionless expansion variable y_p, defined by

$$y_p = y_p(r) = \frac{r^p - r_e^p}{r^p + r_e^p} \qquad (7)$$

where p is a small positive integer ($p = 1, 2, 3, ...$). An important property of the expansion variable y_p is that it remains finite throughout the entire range of the internuclear distance: $y_p = -1$ at $r = 0$, and $y_p = +1$ at $r = \infty$. The function $\phi_{EMO}(r)$ is represented by a simple polynomial in y_p

$$\phi_{EMO}(r) = \sum_{i=0}^{n} \phi_i y_p(r)^i \qquad (8)$$

in which $n = n_S$ for $r \le r_e$, and $n = n_L$ for $r > r_e$. It is sometimes necessary to allow n_S to be smaller than n_L, in order to prevent nonphysical behavior (e.g., potential turnover) in the short-range extrapolation region.[46] The only problem with $n_S < n_L$ is that the overall potential function derivatives of orders larger than $[n_S + 2]$ have small discontinuities at the point $r = r_e$; however, this is not a serious shortcoming because n_S is usually larger

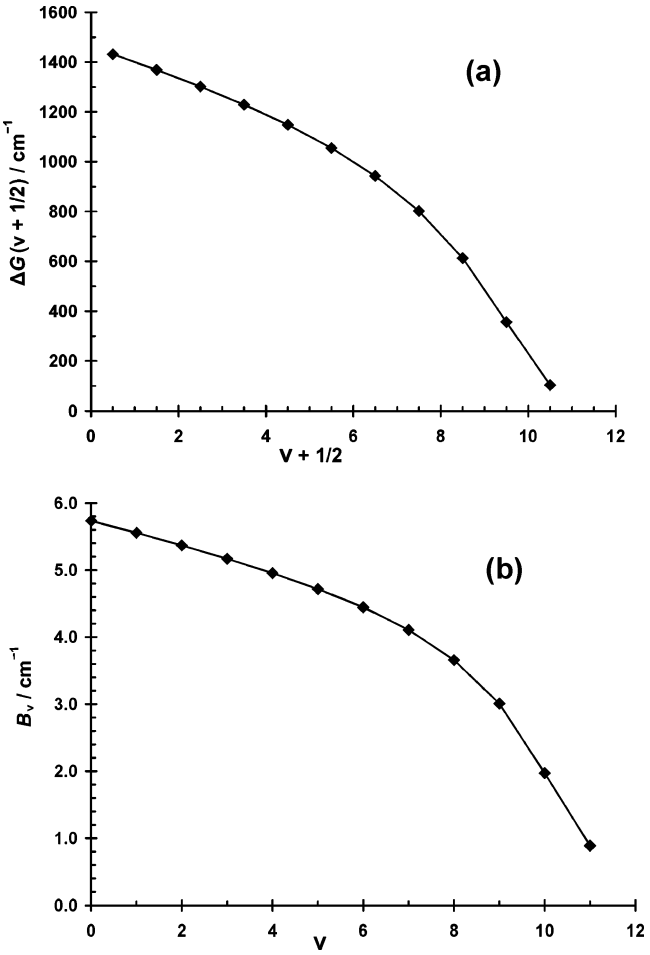

Figure 3. Plots of $\Delta G(v + {}^1/_2)$ and B_v for the $X\,^2\Sigma^+$ ground state of ^{24}MgH.

than three. We denote the EMO potentials by the label EMO$_p$-(n_S, n_L), to express the p value and the order of $\phi_{EMO}(r)$ polynomials used for a particular fit. The flexibility of $\phi_{EMO}(r)$ makes the EMO potential function capable of fitting even very irregular potential energy curves (e.g., see ref 47). However, this function is not constrained to have any specific long-range form, and $\{D_e - V_{EMO}(r)\}$ dies off exponentially at large r.

The second type of analytic potential energy function considered here is the MLR potential, which is formulated to automatically take on the correct form at large internuclear distances. This potential form is defined by the expression

$$V_{ad}(r) = V_{MLR}(r) = D_e\left[1 - \left(\frac{u_{LR}(r)}{u_{LR}(r_e)}\right)e^{-\phi_{MLR}(r)\cdot y_p(r)}\right]^2 \quad (9)$$

in which $u_{LR}(r)$ is the attractive potential at long-range. It is known from theory[51] that the attractive potential energy between any two atoms at long-range ($r \rightarrow \infty$) has the form

$$u_{LR}(r) = \frac{C_{m_1}}{r^{m_1}} + \frac{C_{m_2}}{r^{m_2}} + \cdots \quad (10)$$

and that for our particular case, i.e., the $X\,^2\Sigma^+$ ground state of MgH, the powers m_1 and m_2 are 6 and 8, respectively. The function $\phi_{MLR}(r)$ in eq 9 is represented by the following equation, in which $n = n_S$ for $r \le r_e$, and $n = n_L$ for $r > r_e$:

$$\phi_{MLR}(r) = [1 - y_p(r)]\sum_{i=0}^{n}\phi_i y_p(r)^i + \phi_\infty y_p(r) \quad (11)$$

Therefore, as $r \rightarrow \infty$ we have $\phi_{MLR}(r) = \phi_\infty$, since $y_p(r \rightarrow \infty) = 1$. Hence, as $r \rightarrow \infty$, the overall $V_{MLR}(r)$ potential function collapses to

$$V_{MLR}(r \rightarrow \infty) \approx D_e - \left(\frac{2D_e e^{-\phi_\infty}}{u_{LR}(r_e)}\right)u_{LR}(r) \quad (12)$$

and the correct long-range potential, i.e., $V_{MLR}(r \rightarrow \infty) = D_e - u_{LR}(r)$, is obtained readily by setting $\phi_\infty = \mathrm{Ln}\{2D_e/u_{LR}(r_e)\}$. The major advantage of the MLR potential function[52,53] over the EMO form is that it can provide a much more realistic potential energy function if realistic estimates for the C_m coefficients in eq 10 are available. For the ground state of MgH, values of C_6 and C_8 are available from the theoretical study of Standard and Certain.[51] A special case of the MLR potential function, when only the leading term of the long-range attractive potential in eq 10 is retained, used to be called the Morse/Lennard-Jones (MLJ) potential, and has been utilized in several previous studies.[52−55] In order to distinguish between models that include one versus two terms in the long-range potential, we still use the name MLJ here when only the C_6 constant of MgH is included in $u_{LR}(r)$.

The radial function representing the non-adiabatic centrifugal Born−Oppenheimer breakdown (BOB) correction, $g(r)$ in eq 5, is usually broken into two terms, one for each atom.[56,57] However, since data for only one isotopologue (^{24}MgH) were considered in our analysis, it was impossible to determine separate centrifugal correction functions for the Mg and H atoms. The correction function $g(r)$ for ^{24}MgH was expressed by the following equation in which $\tilde{R}^{Mg}_{na}(r)$ was set to zero:

$$g(r) = \tilde{R}^{Mg}_{na}(r) + \tilde{R}^{H}_{na}(r) = [1 - y_p(r)]\sum_{i=0}^{}t_i^H y_p(r)^i + t_\infty^H y_p(r) \quad (13)$$

The above expression for $g(r)$ is very similar to eq 11 for $\phi_{MLR}(r)$, but the constant t_∞^H is set to zero because by definition there is no nonadiabatic BOB effect as $r \rightarrow \infty$.[56] In addition, the coefficient t_0^H was set to zero, following Watson's convention[58] that $g(r) = 0$ at $r = r_e$. The term $\Delta V_\Sigma(r)$ in eq 5 is similarly expanded as a power series in y_p

$$\Delta V_\Sigma(r) = \frac{\hbar^2}{2\mu r^2}\left\{[1 - y_p(r)]\sum_{i=0}w_i^\Sigma y_p(r)^i + w_\infty^\Sigma y_p(r)\right\} \quad (14)$$

and again the constant w_∞^Σ is set to zero. The integer p used for $g(r)$ or $\Delta V_\Sigma(r)$ in eqs 13 or 14 may in general be different from the one used for the adiabatic potential function, $V_{ad}(r)$. The value of p defining the radial variable in these expressions is simply chosen to ensure that the resulting radial function is well-behaved outside the data region.[56]

The publicly available computer program DPotFit[59] was used for the direct-potential-fit (DPF) analysis. Since the DPF procedure is based on nonlinear least-squares fitting, it requires relatively accurate starting parameters. In the present work, they were obtained in the following manner. First, a Dunham fit was performed for data spanning the vibrational range $v'' = 0-10$ and rotational levels with $N \le 5$. The Dunham $Y_{l,0}$ and $Y_{l,1}$ coefficients were then used to calculate an RKR potential,[60] and the RKR turning points were fitted to EMO and MLR potential

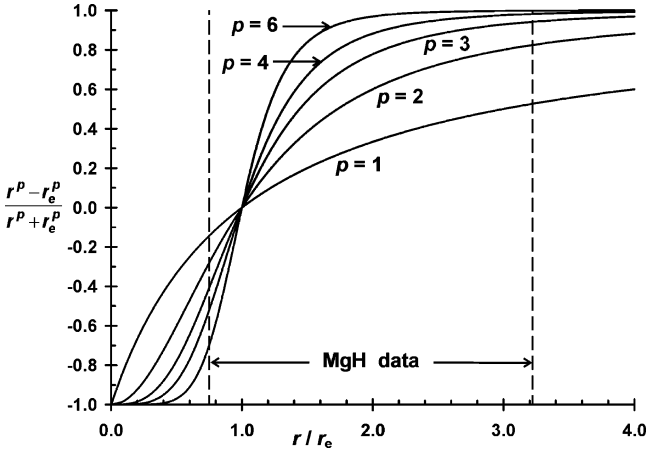

Figure 4. Plots of the expansion variable y_p for different values of p. The MgH data range is defined by the r_{min} and r_{max} turning points of the v″ = 11 level.

forms with various values of p, n_S, and n_L, using program PhiFit.[61] The output parameters (ϕ_i) from program PhiFit were then used as the starting parameters for the DPotFit program. It has been found in previous DPF data analyses that, when $p = 1$ or 2 are used for the y_p expansion variable in eq 7, such fits often have difficulty converging, and the resulting potential functions usually misbehave outside the data region. This was also the case here, as satisfactory fits were only obtained when the radial variable y_p in the exponent coefficient of the adiabatic potential function, eqs 8 and 11, was defined by $p = 3$ or 4. Figure 4 displays plots of the expansion variable y_p for different values of p and the radial range of the MgH experimental data; the inner and outer turning points of the highest vibrational level (v″ = 11) occur at $r_{min} = 1.297$ Å and $r_{max} = 5.574$ Å, respectively. Figure 4 shows that at $p = 4$, for example, the data region covers more than 75% of the entire range of the expansion variable y_p, so the possibility that the function $V_{ad}(r)$ defined in terms of the associated exponent coefficient $\phi(r)$ might exhibit nonphysical behavior outside the data region is greatly reduced. For a detailed discussion about the choice of p values, see refs 46, 52, and 53.

Of the potential function models introduced in this paper, the MLR function provides the most realistic representation of the adiabatic potential, $V_{ad}(r)$, because it incorporates the correct long-range behavior. Theoretical upper and lower bounds for the long-range potential coefficients had been reported by Standard and Certain[51] for a large number of molecules, including MgH. We set the C_6 and C_8 coefficients of the $X\ ^2\Sigma^+$ ground state of MgH to the average of their upper and lower bounds: $C_6 = 2.793 \times 10^5$ cm^{-1} Å^6 and $C_8 = 3.475 \times 10^6$ cm^{-1} Å^8. A major goal of our direct-potential-fit analysis was to obtain the most accurate value possible for the ground state dissociation energy (D_e) of ^{24}MgH, and its estimated uncertainty. In order to obtain an estimate of the maximum degree of model-dependence in the dissociation energy, we performed fits using all three analytic functions, EMO, MLJ, and MLR, with both $p = 3$ and 4 values. The dissociation energy (D_e) and the equilibrium internuclear distance (r_e) were floated in all of these fits, and the results are compared in Table 4. The direct-potential-fit analysis also confirmed that v″ = 11 is the *last* bound level in the $X\ ^2\Sigma^+$ ground state of ^{24}MgH and that it lies only about 13 cm^{-1} below the dissociation asymptote.

For the reasons discussed in the following paragraphs, the MLR$_4$(6,18) function ($p = 4$, $n_S = 6$ and $n_L = 18$) was selected as the best adiabatic potential energy function $V_{ad}(r)$ for the $X\ ^2\Sigma^+$ ground electronic state of ^{24}MgH. We also used eq 13 with $p = 3$ for the nonadiabatic centrifugal correction function $g(r)$, while the spin-rotation interaction potential $\Delta V_\Sigma(r)$ was fitted using eq 14 with $p = 6$. Simultaneously, all the observed energy levels of the $A^2\Pi$ and $B'\ ^2\Sigma^+$ electronic states were fitted as individual term values. Overall, 864 term values were obtained for the sublevels of the $A^2\Pi$ and $B'\ ^2\Sigma^+$ excited states, with average uncertainties of about 0.005 cm^{-1}; they are listed in Table 7S of the Supporting Information. The parameters of our recommended potential and of the associated Hamiltonian radial functions for the $X\ ^2\Sigma^+$ ground state of ^{24}MgH are listed in Table 5. In order to minimize the number of digits required to reproduce the experimental data accurately, the sequential rounding and refitting (SRR) technique[62] was applied to determine the parameters listed in Table 5. First, the values of

TABLE 4: Comparison of Various Potential Functions Used in the Direct-Potential-Fit Analysis of the $X\ ^2\Sigma^+$ Ground State of ^{24}MgH[a]

model[b]	p	n_S	n_L	$\overline{dd}$	D_e/cm^{-1}	r_e/Å
EMO	3	5	16	0.795	11102.7	1.729688
EMO	3	8	17	0.782	11104.6	1.729685
EMO	3	9	17	0.786	11103.1	1.729688
EMO	4	6	17	0.789	11103.5	1.729687
EMO	4	7	18	0.781	11102.8	1.729683
EMO	4	9	18	0.783	11103.1	1.729689
MLJ	3	7	16	0.782	11104.3	1.729683
MLJ	3	8	16	0.789	11104.7	1.729687
MLJ	4	5	18	0.786	11104.2	1.729685
MLJ	4	6	18	0.789	11104.1	1.729681
MLR	3	7	16	0.783	11104.4	1.729683
MLR	3	8	16	0.790	11104.8	1.729687
MLR	4	5	17	0.793	11104.5	1.729675
MLR	4	5	18	0.783	11104.8	1.729684
MLR	**4**	**6**	**18**	**0.783**	**11104.7**	**1.729682**
MLR	4	7	18	0.784	11104.7	1.729679

[a] $\overline{dd}$ is the dimensionless root-mean-square deviation of the fit. [b] The most realistic potential energy function for representing $V_{ad}(r)$ was MLR$_4$(6,18); see the text.

TABLE 5: Parameters of the Recommended MLR$_4$(6,18) Potential Energy Function for the $X\ ^2\Sigma^+$ Ground State of ^{24}MgH, which Represents the Experimental Data with $\overline{dd} = 0.783$[a]

D_e/cm^{-1}	11104.7 ± 0.5	C_6/[cm^{-1} Å^6]	2.793×10^5 (fixed)
r_e/Å	1.729682 ± 0.000005	C_8/[cm^{-1} Å^8]	3.475×10^6 (fixed)
[$p = 4$]		[$p = 3$]	
ϕ_0	−2.33867306	t_0^H	0.0 (fixed)
ϕ_1	−0.7759113	t_1^H	0.0009737(130)
ϕ_2	−1.210606	t_2^H	0.00029(16)
ϕ_3	−0.541097	t_3^H	0.00007(12)
ϕ_4	−0.45237	t_4^H	0.0022(11)
ϕ_5	0.15537	t_5^H	0.0176(18)
ϕ_6	−0.2325	t_6^H	−0.009(1)
$\phi_7/10^3$	2.6224951	t_∞^H	0.0 (fixed)
$\phi_8/10^3$	−52.413692		
$\phi_9/10^3$	476.8244		
$\phi_{10}/10^3$	−2595.56525	[$p = 6$]	
$\phi_{11}/10^3$	9372.1667	w_0^Σ	0.0046212(6)
$\phi_{12}/10^3$	−23536.146	w_1^Σ	0.002228(84)
$\phi_{13}/10^3$	41909.27	w_2^Σ	0.00262(7)
$\phi_{14}/10^3$	−52887.07	w_3^Σ	0.0024(3)
$\phi_{15}/10^3$	46342.3	w_∞^Σ	0.0 (fixed)
$\phi_{16}/10^3$	−26852.		
$\phi_{17}/10^3$	9260.		
$\phi_{18}/10^3$	−1440.		

[a] The numbers in parentheses are 2σ standard deviation uncertainties in the last quoted digits. The uncertainties in D_e and r_e are based on model-dependence.

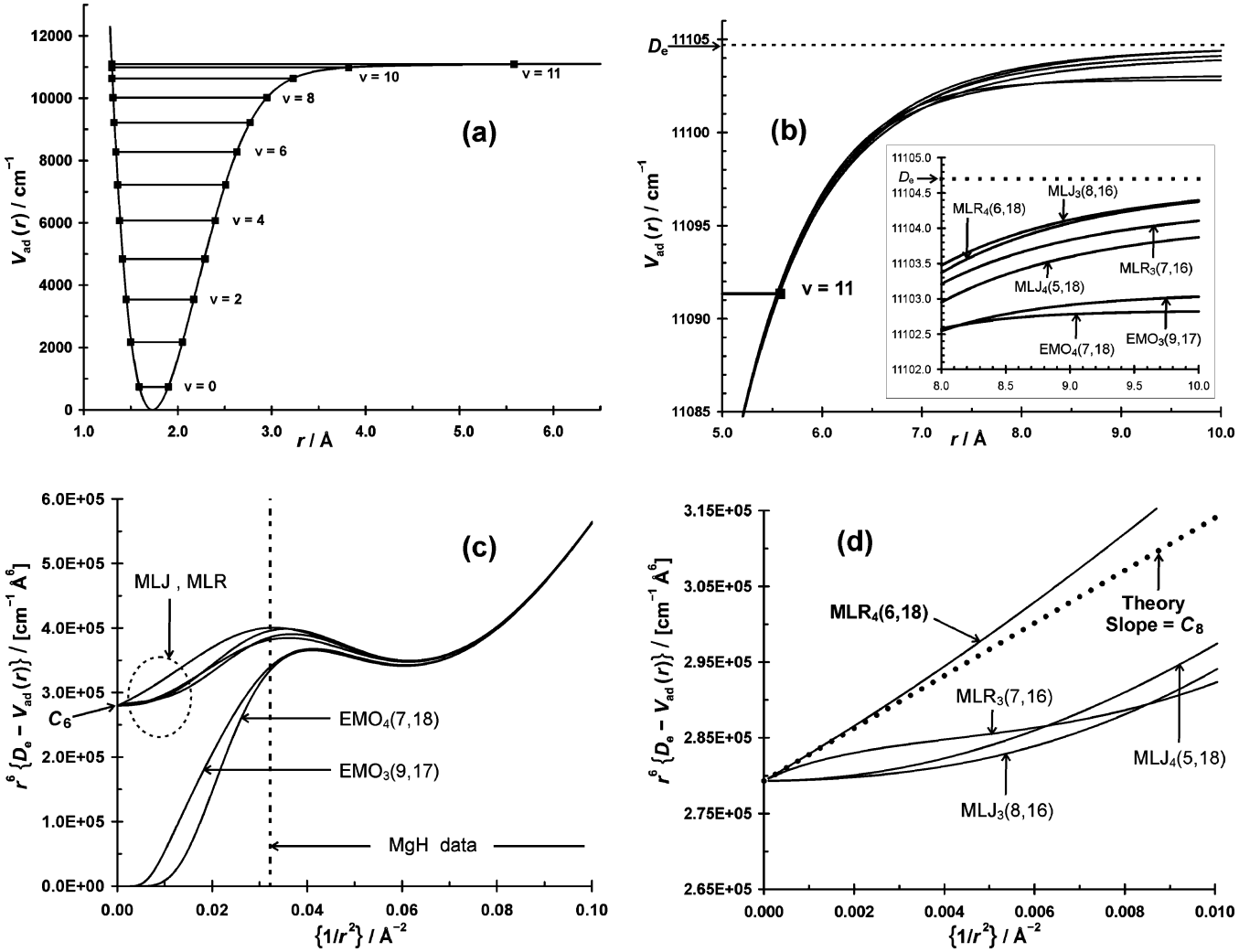

Figure 5. (a) Adiabatic potential energy function for the $X\,^2\Sigma^+$ ground electronic state of ^{24}MgH, based on the MLR$_4$(6,18) model. (b) The differences between various potential functions in the extrapolation region. (c) The long-range behavior of the EMO, MLJ and MLR potential functions. (d) The MLJ and MLR potentials at $r \rightarrow \infty$, compared with the theoretical prediction.

r_e and D_e were rounded manually, based on their statistical uncertainties; the rest of the parameters were then rounded automatically using the SRR technique. The resulting recommended adiabatic potential energy function for the $X\,^2\Sigma^+$ ground electronic state of ^{24}MgH is plotted in Figure 5a. The adiabatic potential energy functions obtained from EMO and MLJ models differ very slightly from the MLR$_4$(6,18) potential. These differences mostly appear outside the data region, i.e., at energies higher than the v = 11 level, where all potential functions approach the dissociation asymptote. The differences among the various potential functions in the "extrapolation region" are illustrated in Figure 5b.

The correct long-range attractive potential for the $X\,^2\Sigma^+$ ground state of ^{24}MgH is given by eq 10, with m_1 and m_2 set equal to 6 and 8, respectively. Therefore, in a plot of $r^6\{D_e - V_{ad}(r)\}$ versus $1/r^2$, the y intercept should be equal to C_6, the slope as $\{1/r^2\} \rightarrow 0$ should be equal to C_8, and the plot should approach the slope from above, since the leading correction to our two-term $u_{LR}(r)$ function (eq 10) should be an attractive C_{10}/r^{10} term. This is certainly not the case for the EMO potentials because $\{D_e - V_{EMO}(r)\}$ dies off exponentially at large r. The MLJ potential, on the other hand, is constrained to have the correct intercept (C_6), but not the correct slope at this intercept. The plots of $r^6\{D_e - V_{ad}(r)\}$ versus $1/r^2$ for a number of potential functions from Table 4 are displayed in Figure 5. By definition, the MLR function is constrained to have both intercept and slope defined by the theoretical C_6 and C_8 coefficients, and should give the most realistic adiabatic potential energy. As illustrated in Figure 5, panels c and d, the MLR$_4$-(6,18) model represents the long-range potential energy correctly, and joins it to the short-range potential very smoothly. Therefore, the MLR$_4$(6,18) function was selected as the best function for $V_{ad}(r)$.

In order to illustrate the effect of the centrifugal potential, i.e., the third term in the Hamiltonian operator in eq 5, the total potential energy $\{V_{ad}(r) + V_{cent}(r)\}$ has been plotted in Figure 6 for some values of the rotational quantum number, N. This figure shows that at $N = 50$, for example, only the v = 0−2 levels exist, and they are all quasibound. Plots of the exponent function $\phi_{MLR}(r)$ of the recommended MLR$_4$(6,18) potential, of the nonadiabatic centrifugal BOB correction function $g(r)$, and of the spin-rotation interaction potential $\Delta V_\Sigma(r)$ are also shown in Figure 6. Outside the data region, these radial functions remain well-behaved and display no nonphysical behavior.

Although the tunneling predissociation widths (Table 2) were included as additional data in our data set, we found that they had no significant effect on the fitted values of the dissociation energy or other potential parameters. In addition, Table 4 shows that even the nonconstrained EMO potentials give dissociation energies that are fairly close to those obtained from fits to the more realistic MLJ and MLR potentials. In other words, even if there had been no information on the long-range C_6 and C_8

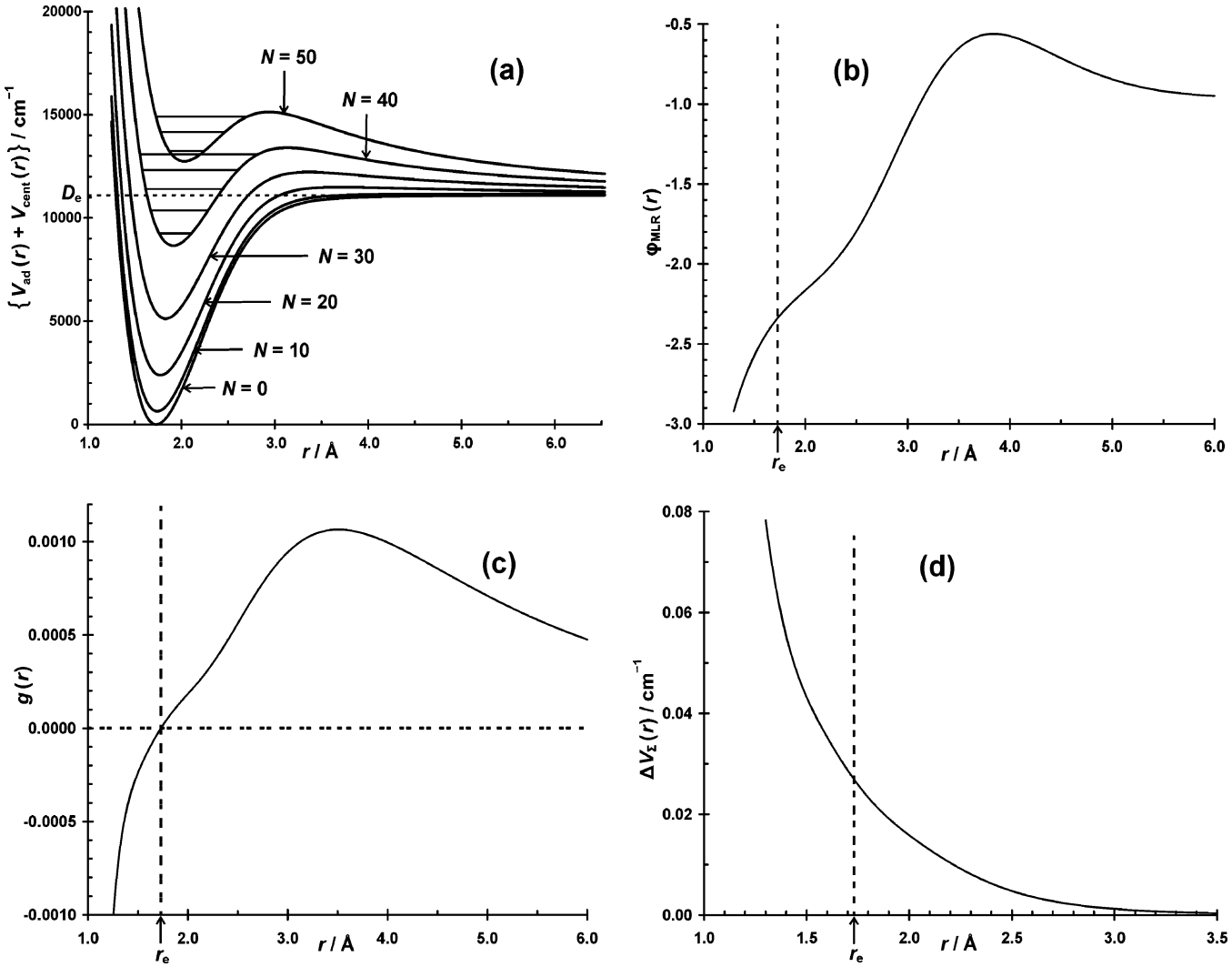

Figure 6. (a) Total potential energy $\{V_{ad}(r) + V_{cent}(r)\}$ for different rotational quantum numbers, $N = 0$, 10, 20, 30, 40, and 50. (b) Plot of the radial function $\phi_{MLR}(r)$ from the recommended $MLR_4(6,18)$ potential. (c) The radial correction function $g(r)$ for the non-adiabatic Born-Openheimer breakdown effects. (d) The spin-rotation interaction potential $\Delta V_\Sigma(r)$.

coefficients, the dissociation energy would have been underestimated by less than 2 cm^{-1}. The main reason for the high precision and consistency in the dissociation energy of ^{24}MgH is that all of the bound vibrational levels have been observed experimentally, and the extrapolation region is very small, i.e., less than 14 cm^{-1} from the $v = 11$ level to the asymptote. On the basis of its model-dependence, we estimated an overall uncertainty of about 0.5 cm^{-1} for D_e; in estimating the contribution of model-dependence to this quantity, we considered only the various MLJ and MLR models of Table 4, because the EMO potentials approach the dissociation asymptote exponentially, and thus underestimate D_e systematically. As a final check on our estimated uncertainty in D_e, we used the upper and lower limits of the theoretical C_6 and C_8 coefficients[51] for the $MLR_4(6,18)$ fit. The discrepancies between the D_e values obtained from these fits and the one listed in Table 5 were less than ± 0.1 cm^{-1}. Therefore, we report the equilibrium dissociation energy for the $X\,^2\Sigma^+$ ground electronic state of ^{24}MgH to be $D_e = 11\,104.7 \pm 0.5$ cm^{-1} from the $MLR_4(6,18)$ potential. The zero-point energy, i.e., the vibrational energy of the $v'' = 0$ level relative to the bottom of the potential curve, was determined to be 739.11 cm^{-1}, which varied only by ± 0.01 cm^{-1} among different models. Therefore, the zero-point dissociation energy is $D_0 = 10\,365.6 \pm 0.5$ cm^{-1}. The equilibrium internuclear distance (r_e) from the $MLR_4(6,18)$ fit is 1.729682 Å and has an estimated uncertainty of $\pm$ 0.000005 Å, most of which is due to model-dependence.

A list of band constants, i.e., G_v, B_v, and six centrifugal distortion constants, were generated automatically by the DPotFit program (Table 6S). These parameters have real physical significance, unlike the band constants obtained from the empirical fit. However, they cannot reproduce the very high N rotational energy levels accurately, because yet higher-order centrifugal distortion constants (more than six) are required. The G_v, B_v, and D_v constants and turning points r_{min} and r_{max} listed in Table 3 have been calculated from the recommended $MLR_4(6,18)$ potential energy function and not from the empirical fits. Since both band-constant and Dunham fits result in parameters that are mechanically inconsistent, the best way to reproduce all of the observed energy levels of the $X\,^2\Sigma^+$ ground state is by using the recommended $MLR_4(6,18)$ potential energy function and solving eq 5, i.e., the radial Schrödinger equation, numerically. We generated a list of all the vibration−rotation energy levels (term values) of the $X\,^2\Sigma^+$ ground state of ^{24}MgH by using the complete potential energy function, including $g(r)$ and $\Delta V_\Sigma(r)$, in the DPotFit program; see Table 8S in the Supporting Information. This list also includes some very high N rotational levels that were not observed in our spectra.

Discussion and Conclusions

The band-constant fit for the $X\,^2\Sigma^+$ ground state was useful for confirming the rotational assignments of the electronic bands and required 101 empirical parameters. The Dunham fit required 107 parameters and yielded many high-order polynomial coefficients with no physical significance. During the first steps of data analysis, the ground state vibrational levels up to $v'' = 10$ were assigned, and the results of a Dunham fit suggested that the $v'' = 11$ level is not bound. However, near dissociation expansion (NDE)[63] fits to the vibrational energies, G_v, of the $v'' = 0$ to 10 levels predicted that the $v'' = 11$ level is bound, and that the $v'' = 11 \rightarrow 10$ interval is about 79 cm^{-1}. On the other hand, a preliminary direct-potential-fit (DPF) analysis of the $v'' = 0-10$ data with the MLJ model predicted the $v'' = 11 \rightarrow 10$ interval to be 103 cm^{-1}, significantly larger than that of the NDE fit. With the help of the MLJ potential predictions, the $v'' = 11$ was found in the $B'\,^2\Sigma^+ \rightarrow X\,^2\Sigma^+$ spectrum, and the 3−11 band was assigned up to $N'' = 3$. The observed $v'' = 11 \rightarrow 10$ interval turned out to be 102.84 cm^{-1}, remarkably close to the predicted value from the preliminary DPF analysis. This indicates the great advantage of DPF method over empirical Dunham fits for predicting unobserved energy levels, especially for levels close to the dissociation asymptote. Moreover, to achieve the same quality of fit, the DPF analysis required less than one-third as many free parameters as did the "parameter fit" analyses.

The nonadiabatic BOB effects in the centrifugal potential were accounted for by $g(r)$, which is a dimensionless function of the internuclear distance. As seen in Figure 6c, the maximum value of $g(r)$ in the data region is about 0.001, but a sixth-order polynomial in y_p was required for fitting this function. This is a direct consequence of the existence of high-quality data at very large N values. We also note that since the data for only one isotopologue (^{24}MgH) were considered in our analysis, the determination of separate centrifugal BOB functions for the Mg and H atoms was not possible. Therefore, the small BOB effects from the Mg atom are hidden inside the t_i^H parameters. We are in the process of analyzing similar visible spectra for MgD, and we will ultimately perform a multi-isotopologue DPF analysis for this molecule.

The equilibrium dissociation energy for the $X\,^2\Sigma^+$ ground electronic state of ^{24}MgH was determined to be $D_e = 11\,104.7 \pm 0.5$ cm^{-1}, and the equilibrium internuclear distance was found to be $r_e = 1.729682 \pm 0.000005$ Å. The zero-point energy, i.e., the vibrational energy of the $v'' = 0$ level relative to the bottom of the potential curve, is 739.11 ± 0.01 cm^{-1}. Therefore, the zero-point dissociation energy is $D_0 = 10\,365.6 \pm 0.5$ cm^{-1}. Our estimated uncertainties in these quantities are based on model-dependence, and are significantly larger than the statistical uncertainties associated with the parameter values determined in the fits. The individual energy levels (term values) of the $A^2\Pi$ and $B'\,^2\Sigma^+$ states were determined with uncertainties of about 0.005 cm^{-1} and were listed in Table 7S. A deperturbation analysis of the $A^2\Pi$ and $B'\,^2\Sigma^+$ energy levels has just been completed and will be published elsewhere. MgH is now the only hydride molecule other than H_2 itself for which all bound vibrational levels of the ground electronic state are observed experimentally and for which the dissociation energy is determined with subwavenumber accuracy.

Acknowledgment. Financial support for this work was provided by the Natural Sciences and Engineering Research Council (NSERC) of Canada through Discovery Grants to P.F.B. and R.J.L. and through an undergraduate student research award (USRA) to R.D.E.H.

Supporting Information Available: A complete list of data, spectroscopic constants, and energy levels of ^{24}MgH (Tables 1S−9S). This material is available free of charge via the Internet at http://pubs.acs.org.

References and Notes

(1) Fowler, A. *Mon. Not. R. Astron. Soc.* **1907**, *67*, 530.
(2) Fowler, A. *Phil. Trans. R. Soc. London A* **1909**, *209*, 447.
(3) Sotirovski, P. *Astron. Astrophys. Suppl.* **1972**, *6*, 85.
(4) Wallace, L.; Hinkle, K.; Li, G.; Bernath, P. F. *Astrophys. J.* **1999**, *524*, 454.
(5) Kirkpatrick, J. D. *Annu. Rev. Astron. Astrophys.* **2005**, *43*, 195.
(6) Boesgaard, A. M. *Astrophys. J.* **1968**, *154*, 185.
(7) Gay, P. L.; Lambert, D. L. *Astrophys. J.* **2000**, *533*, 260.
(8) Watson, W. W.; Rudnick, P. *Astrophys. J.* **1926**, *63*, 20.
(9) Watson, W. W.; Rudnick, P. *Phys. Rev.* **1927**, *29*, 413.
(10) Mulliken, R. S. *Phys. Rev.* **1928**, *32*, 388.
(11) Pearse, R. W. B. *Proc. R. Soc. A* **1928**, *122*, 442.
(12) Fujioka, Y.; Tanaka, Y. *Sci. Pap. Inst. Phys. Chem. Res.* **1936**, *30*, 121.
(13) Grundström, B. *Nature* **1936**, *137*, 108.
(14) Guntsch, A. *Z. Phys.* **1937**, *104*, 584.
(15) Turner, L. A.; Harris, W. T. *Phys. Rev.* **1937**, *52*, 626.
(16) Guntsch, A. *Z. Phys.* **1937**, *107*, 420.
(17) Huber, K. P.; Herzberg, G. *Molecular Spectra and Molecular Structure IV. Constants of Diatomic Molecules*; Van Nostrand: New York, 1979.
(18) Balfour, W. J. *Astrophys. J.* **1970**, *162*, 1031.
(19) Balfour, W. J. *J. Phys. B: Atom. Mol. Phys.* **1970**, *3*, 1749.
(20) Balfour, W. J.; Cartwright, H. M. *Chem. Phys. Lett.* **1975**, *32*, 82.
(21) Balfour, W. J.; Cartwright, H. M. *Can. J. Phys.* **1975**, *53*, 1477.
(22) Balfour, W. J.; Cartwright, H. M. *Can. J. Phys.* **1976**, *54*, 1898.
(23) Balfour, W. J.; Cartwright, H. M. *Astron. Astrophys. Suppl.* **1976**, *26*, 389.
(24) Balfour, W. J.; Lindgren, B. *Can. J. Phys.* **1978**, *56*, 767.
(25) Balfour, W. J. *J. Mol. Spectrosc.* **1980**, *79*, 507.
(26) Bernath, P. F.; Black, J. H.; Brault, J. W. *Astrophys. J.* **1985**, *298*, 375.
(27) Lemoine, B.; Demuynck, C.; Destombes, J. L.; Davies, P. B. *J. Chem. Phys.* **1988**, *89*, 673.
(28) Leopold, K. R.; Zink, L. R.; Evenson, K. M.; Jennings, D. A.; Mizushima, M. *J. Chem. Phys.* **1986**, *84*, 1935.
(29) Zink, L. R. Ph.D. Thesis; University of Colorado, 1986.
(30) Zink, L. R.; Jennings, D. A.; Evenson, K. M.; Leopold, K. R. *Astrophys. J.* **1990**, *359*, L65.
(31) Ziurys, L. M.; Barclay, W. L. Jr.; Anderson, M. A. *Astrophys. J.* **1993**, *402*, L21.
(32) Shayesteh, A.; Appadoo, D. R. T.; Gordon, I.; Le Roy, R. J.; Bernath, P. F. *J. Chem. Phys.* **2004**, *120*, 10002.
(33) Meyer, W.; Rosmus, P. *J. Chem. Phys.* **1975**, *63*, 2356.
(34) Sink, M. L.; Bandrauk, A. D.; Henneker, W. H.; Lefebvre-Brion, H.; Raseev, G. *Chem. Phys. Lett.* **1976**, *39*, 505.
(35) Saxon, R. P.; Kirby, K.; Liu, B. *J. Chem. Phys.* **1978**, *69*, 5301.
(36) Kirby, K.; Saxon, R. P.; Liu, B. *Astrophys. J.* **1979**, *231*, 637.
(37) Sink, M. L.; Bandrauk, A. D. *Can. J. Phys.* **1979**, *57*, 1178.
(38) Weck, P. F.; Schweitzer, A.; Stancil, P. C.; Hauschildt, P. H.; Kirby, K. *Astrophys. J.* **2003**, *582*, 1059.
(39) Weck, P. F.; Stancil, P. C.; Kirby, K. *Astrophys. J.* **2003**, *582*, 1263.
(40) Weck, P. F.; Schweitzer, A.; Stancil, P. C.; Hauschildt, P. H.; Kirby, K. *Astrophys. J.* **2003**, *584*, 459.
(41) Skory, S.; Weck, P. F.; Stancil, P. C.; Kirby, K. *Astrophys. J. Suppl. Ser.* **2003**, *148*, 599.
(42) Hirao, T.; Pinchemel, B.; Bernath, P. F. *J. Mol. Spectrosc.* **2000**, *202*, 213.
(43) Norlen, G. *Phys. Scr.* **1973**, *8*, 249.
(44) Whaling, W.; Anderson, W. H. C.; Carle, M. T.; Brault, J. W.; Zarem, H. A. *J. Res. Natl. Inst. Stand. Technol.* **2002**, *107*, 149.
(45) Bernath, P. F. *Spectra of Atoms and Molecules*, 2nd ed.; Oxford University Press: New York, 2005.
(46) Huang, Y.; Le Roy, R. J. *J. Chem. Phys.* **2003**, *119*, 7398.
(47) Le Roy, R. J.; Appadoo, D. R. T.; Anderson, K.; Shayesteh, A.; Gordon, I .E.; Bernath, P. F. *J. Chem. Phys.* **2005**, *123*, 204304.
(48) Dunham, J. L. *Phys. Rev.* **1932**, *41*, 713.
(49) Dunham, J. L. *Phys. Rev.* **1932**, *41*, 721.
(50) Morse, P. M. *Phys. Rev.* **1929**, *34*, 57.
(51) Standard, J. M.; Certain, P. R. *J. Chem. Phys.* **1985**, *83*, 3002.
(52) Le Roy, R. J.; Huang, Y.; Jary, C. *J. Chem. Phys.* **2006**, *125*, 164310.
(53) Le Roy, R. J.; Henderson, R. D. E. *Mol. Phys.* **2007**, *105*, 691.

(54) Hajigeorgiou, P. G.; Le Roy, R. J. *J. Chem. Phys.* **2000**, *112*, 3949.
(55) Seto, J. Y.; Le Roy, R. J.; Vergès, J.; Amiot, C. *J. Chem. Phys.* **2000**, *113*, 3067.
(56) Le Roy, R. J.; Huang, Y. *J. Mol. Struct. (THEOCHEM)* **2002**, *591*, 175.
(57) Le Roy, R. J.; Appadoo, D. R. T.; Colin, R.; Bernath, P. F. *J. Mol. Spectrosc.* **2006**, *236*, 178.
(58) Watson, J. K. G. *J. Mol. Spectrosc.* **2004**, *223*, 39.
(59) Le Roy, R. J. *DPotFit 1.2*; University of Waterloo Chemical Physics Research Report CP-662R, 2007; http://leroy.uwaterloo.ca.
(60) Le Roy, R. J. *RKR1 2.0*; University of Waterloo Chemical Physics Research Report CP-657, 2003; http://leroy.uwaterloo.ca.
(61) Le Roy, R. J. *PhiFit 1.2*; University of Waterloo Chemical Physics Research Report CP-663R, 2007; http://leroy.uwaterloo.ca.
(62) Le Roy, R. J. *J. Mol. Spectrosc.* **1998**, *191*, 223.
(63) Le Roy, R. J.; Lam, W.-H. *Chem. Phys. Lett.* **1980**, *71*, 544.